Regular Article

PHYSICAL CHEMISTRY RESEARCH
Published by the
Iranian Chemical Society
www.physchemres.org
info@physchemres.org

Phys. Chem. Res., Vol. 12, No. 1, 229-248, March 2024
DOI: 10.22036/pcr.2023.386259.2294

Theoretical and Experimental Study of the Orientation to the Most Effective Coagulant for Removing Reactive Black-5 Dye from Industrial Effluents

S. El Harfaoui[a], Z. Zmirli[b], A. Mohssine[a], A. Dani[a], B. Sallek[b], A. Tounsi[c], K. Digua[a], M. El Idrissi[d,*] and H. Chaair[a]

[a]*Laboratory of Process Engineering and Environment, Faculty of Sciences and Technology Mohammedia, B.P 577. Univ. Hassan II, Casablanca, Morocco*

[b]*Laboratory of Advanced Materials and Process Engineering, Faculty of Sciences Kenitra, Univ. Ibn Tofail, B.P 133, Kénitra, Morocco*

[c]*Agro-Industrial, Environmental and Ecological Processes Team, Faculty of Science and Technology, Sultan Moulay Slimane University, Morocco*

[d]*Team of Chemical Processes and Applied Materials, Sultan Moulay Slimane University, Polydisciplinary Faculty of Beni-Mellal, B.P 23000 Morocco*

(Received 18 February 2023, Accepted 25 June 2023)

The current research was designed to provide a theoretical approach for the selection of the optimum coagulant to remove Reactive Black-5 dye from industrial waste. Additionally, it seeks to identify the dye's most reactive sites and understand its degradation in water pollution. Theoretically, the study was investigated using the density functional theory (DFT) with a 6-31G(d) basis set. The studied molecules are the reactive Black-5 dye, ferric sulphate ($Fe_2(SO_4)_3$), ferric chloride ($FeCl_3$), aluminium sulphate ($Al_2(SO_4)_3$), and aluminium chloride ($AlCl_3$). Based on the electrophilicity index, the results revealed the following classification: $Fe_2(SO_4)_3 > FeCl_3 > Al_2(SO_4)_3 > AlCl_3$. Thus, $Fe_2(SO_4)_3$ acts as an electrophile, and the Reactive (RB5) as a nucleophile. The Parr index analysis of the dye studied indicates that the most vulnerable region for the nucleophilic attack is sited on the C5-9H bonding area with $\omega_k = 2.797$ eV. The results of the experiments match well with the reported theoretical data, with the coagulant $Fe_2(SO_4)_3$ achieving the highest Chemical Oxygen Demand removal rate (84.71% at pH = 4). To support the findings, we provide an experimental investigation using the coagulation-flocculation method for these various coagulants to remove the reactive Black-5 dye from industrial effluents.

Keywords: DFT investigation, Dye removal, Coagulation, Electrophilicity index, Reactivity descriptors

INTRODUCTION

The dyes are a coloring substances employed in numerous domains, including the printing, leather, paper, textile, and cardboard packaging industries [1]. Additionally, each year, 700,000 tonnes of dyes, of which 60-70% are azo dyes, are produced worldwide in more than 100,000 different commercially accessible dye variants [2,3]. Because of their composition, complex aromatic structure, natural stability [4], and release, these dyes pose a constant and severe environmental risk. These chemical substances negatively impact aquatic fauna and flora [5,6]. Therefore, substantial efforts are deployed to perform effective treatments. In addition, different dye-removing strategies have been developed in numerous investigations, which all claim to be effective in removing dyes [7-13]. This has provided a better understanding of the process at a macro level. Several previous studies have shown that coagulation-flocculation treatment is extensively employed because of its lower price, higher accessibility, and ease of processing [14,15]. Classically, it is based on many experimental tests on different coagulants to determine which coagulant is most

*Corresponding author. E-mail: m.elidrissi2018@gmail.com

efficient in achieving the highest performance in removing the pollutant load from wastewater. However, there are some drawbacks to using this method, including the investment of time and resources, reagents, potential inaccuracies in selecting coagulants, and occasional imprecision in operating conditions.

To overcome these inconveniences, we have applied the conceptual density functional theory (CDFT) of molecules as an innovative approach to industrial wastewater treatment. This theory has been developed at the beginning of the 21st century and is based on the calculation of quantum chemistry applied to a molecular system. Moreover, this theoretical approach allows us to obtain essential data concerning the molecular system (structural nature, energetic, electronic, *etc*.). When properly analyzed, verified, and interpreted, these properties allow us to understand and anticipate the system's reactivity. Furthermore, they predict the reaction mechanisms between different reagents and determine the best combination. Thus, over the last 20 years, in most areas of chemistry and materials science, CDFT based on theoretical reactivity indices has emerged as a valuable and instructive guide for analyzing organic reactivity and defining intermolecular interactions [16]. Various reactivity indices have been reported in the bibliography, and several experimental investigations in organic and inorganic chemistry are now being conducted. These studies include calculations using a standard basis set and functional approximation [17-19]. Therefore, several studies were inspired by the DFT approach to predict the reactivity in different media and by other dye removal techniques before starting the experimental protocols. Recent DFT studies demonstrate that removal effectiveness is directly correlated with electrophilicity, according to quantum chemistry data [20-22]. Also, it allows for the prediction of the efficiency and attack sites of the molecule to be treated, which aids and facilitates the selection of reagents even before the experimental tests begin. Likewise, the DFT calculations were used to analyze and predict the reaction between the reagent and the dye molecule, [21,23-24].

The present work provides a theoretical study on the reaction involving Reactive Black-5 (RB5) dye and four different reagents: ferric sulphate ($Fe_2(SO_4)_3$), ferric chloride ($FeCl_3$), aluminium sulphate ($Al_2(SO_4)_3$), and aluminium chloride ($AlCl_3$). The main aim is to identify the most effective coagulant for removing the Reactive Black 5 dye. Furthermore, this investigation explores the potential of DFT as a powerful tool to determine the sites or atoms responsible for nucleophilic or electrophilic attacks by exploiting the precision of DFT in predicting the reactivity of reagents.

The present study includes the following results:

- Optimization of the geometries of various studied molecules using DFT/6-31G(d) and calculating their reactivity descriptors. This basis set has been selected by comparing the experimental absorption wavelength of the RB5 dye and the theoretical wavelength values calculated using different basis sets (DFT/B3LYP/6-31G(d), 6-31+G(d), 6-31G(d,p), 6-31+G(d,p), 6-31++G(d,p), and 3-21G(d,p));
- Reactivity analysis of the reactive black-5 dye and the four coagulants using DFT's global and local reactivity descriptors. These descriptors can be used to predict the reactivity behavior of chemical systems;
- Determination of the preferred nucleophilic or electrophilic attack sites;
- Elaboration of a theoretical classification of the coagulants studied according to their affinities to react with the reagent reactive black-5 dye;
- Conduction of an experimental study to determine the effectiveness of removing wastewater that contains RB5. Later, we analyzed and contrasted the outcomes of our experiments with the corresponding theoretical data.

THEORETICAL STUDY

Characterization of the Reactive Black-5 Dye and Reagents

Reactive Black-5 dye, a commercial product, was used in this research. Table 1 displays the properties of the RB5, including its chemical class, molecular weight, molecular formula, $C_{26}H_{21}N_5Na_4O_{19}S_6$, and maximum absorption wavelength.

In this study, four coagulants were employed being ferric sulphate ($Fe_2(SO_4)_3$), ferric chloride ($FeCl_3$), aluminium sulphate ($Al_2(SO_4)_3$), and aluminium chloride ($AlCl_3$). The summary of coagulant characteristics is presented in Table 2.

Computational Methods

The absorbances were performed using a spectrophotometer of the Type U-5100 UV-Vis (Hitachi, Japan) apparatus.

Table 1. Characteristics of Reactive Black-5 Dye [25]

Parameter	Value
Chemical class	Azo
C.I. Name	Remazol Black 5
Commercial name	Reactive Black 5
Molecular weight (g mol^{-1})	991.82
Molecular formula	$C_{26}H_{21}N_5Na_4O_{19}S_6$
Wavelength absorbed (nm)	597
Solubility	200 g l^{-1} in water at 80 °C
Composition	≥50% of dye content
pH of the stock solution	5.5

Table 2. Characteristics of Coagulants Used in the Experiments

	Ferric sulfate	Ferric chloride	Aluminum sulfate	Aluminum chloride
Appearance	Yellow crystalline solid or a grayish-white powder	Orange to brown-black solid	White crystalline solid hygroscopic	White or pale-yellow Solid, hygroscopic
Density (g cm^{-3})	3.1	2.9	2.672	2.48
Viscosity		-	-	0.35
Optimal pH	3-5	4-6	6-9	9-11
Molecular weight	399.9 (g mol^{-1})	162.20 (g mol^{-1})	342.2 (g mol^{-1})	133.341 (g mol^{-1})

Figure 1 displays the UV-Vis spectrum of RB5 dye in an aqueous solution obtained from the experiment. The experimental spectrum has two strong absorbance peaks at 310 and 588 nm. For RB5 dye, it is observed that the wavelength corresponding to the maximum absorbance, λ_{max} occurs at 588 nm.

To determine the most suitable basis set for studying the RB5 dye, we have computed the theoretical absorption wavelength values for the RB5 dye using six different basis sets at DFT/B3LYP/6-31G(d), 6-31+G(d), 6-31G(d,p), 6-31+G(d,p), 6-31++G(d,p), and 3-21G(d,p) levels. The calculations were carried out using Gaussian 09 software. Figure 2 shows the computed wavelength (λ_{max}) for all basis sets used with the DFT/B3LYP function compared to the experimental value.

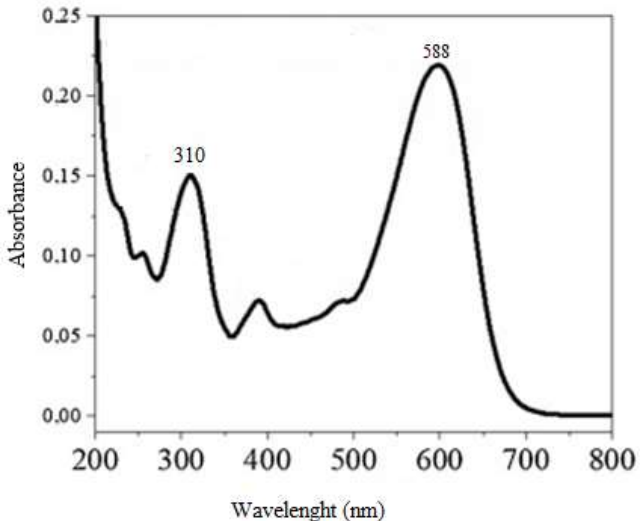

Fig. 1. Experimental UV-Vis spectrum of RB5 dye.

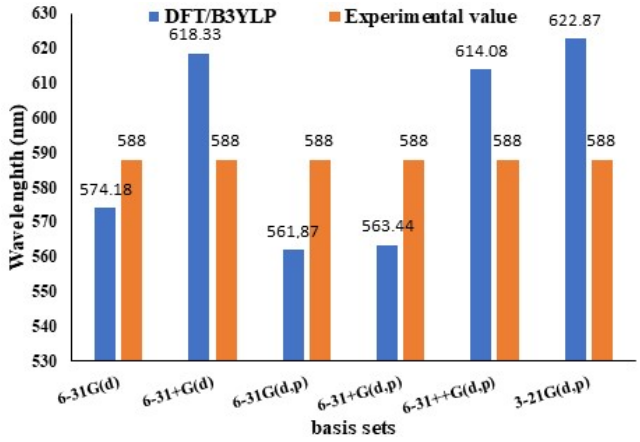

Fig. 2. Comparison of the theoretical and experimental values of the absorbance wavelength for the RB5 dye.

After analyzing the data, it is important to note that each basis set yields distinct theoretical values for the wavelength absorbance. Based on the theoretical and experimental data, it can be concluded that the DFT/B3LYP/6-31G(d) basis set provides a wavelength absorbance value of 574.18 nm, which is close to the experimental absorbance value of RB5 dye (588 nm) (Fig. 1). Therefore, this base set is the most appropriate to study the geometry optimization and calculations for the RB5 dye. Furthermore, the 6-31G(d) basis calculations are similar to those of the 6-31G set basis. This result is in good agreement with a previous study on the effect of adding polarization. It has been revealed that this function does not significantly improve the calculation of excitation energies [26].

Materials and Methods

The Density Functional Theory is performed using the Gaussian 09W program [27,28], taking into account the standard convergence criteria established in the software package. The Becke3-Lee-Yang-Parr functional with a (B3LYP,6-31G(d)) basis set was used to optimize the geometry of the RB5 dye, and the $FeCl_3$, $Fe_2(SO_4)_3$, $Al_2(SO_4)_3$, and $AlCl_3$ coagulants [21] [29,30].

The Natural Bond Orbital (NBO) analysis has been utilized to investigate the electronic properties of these molecules. We evaluated the global and local descriptors of the optimized molecules by subjecting them to single-point computations. Specific variables have a substantial impact on chemical reactivity. These variables are commonly observed as the eigenvalues of the energy of the highest occupied molecular orbital (E_{HOMO}), the energy of the lowest unoccupied molecular orbital (E_{LUMO}), energy gap (ΔE_{gap}), ionization energy (IE) (Eq. (1)), electron affinity (EA) (Eq. (2)), absolute electronegativity (χ), global hardness (η), global softness (S), global electrophilicity index (ω), the electroaccepting, ω^+, and electrodonating, ω^- [31] and a fraction of electrons transferred (ΔN_{max}) [32]. In chemical reactions, we utilize the HOMO and LUMO energies as descriptors to compute global indexes within the DFT framework.

The IE and EA can come from the difference between neutral and cation for IE and neutral and anion for EA [33,34]. The ionization energy and the electron affinity were determined using the following Eqs. (1) and (2):

$$IE = E(N-1) - E(N) \quad (1)$$

and

$$EA = E(N) - E(N+1) \quad (2)$$

Where: (N) is the energy for the neutral, (N-1) is the energy for the cation, and (N+1) denotes the energy for the anion.

The energy difference (E_{gap}) between the lowest unoccupied molecular orbital (E_{LUMO}) and the highest occupied molecular orbital (E_{HOMO}) is the gap energy, which is given by Eq. (3).

$$\Delta E_{gap}(eV) = E_{LUMO} - E_{HOMO} \quad (3)$$

The absolute chemical hardness was computed using Eq. (4) [35].

$$\eta = \frac{IE-AE}{2} = \frac{E_{LUMO}-E_{HOMO}}{2} \quad (4)$$

The chemical softness, as stated in Eq. (5), describes an atom or a group of atom's abilities to receive electrons.

$$S = \frac{1}{\eta} = \frac{2}{E_{HOMO}-E_{LUMO}} \quad (5)$$

The electronegativity, χ referred to μ as the chemical potential's negative in the finite difference approximation,

being a component of the overall reactivity. The electronegativity was determined using Eq. (6).

$$\chi = \frac{IE+AE}{2} = \frac{-(E_{LUMO}+E_{HOMO})}{2} \quad (6)$$

From the molecular orbital energies E_{HOMO}/E_{LUMO} borders, the electronic chemical potential is computed as follows:

$$\mu = \frac{E_{LUMO}+E_{HOMO}}{2} \quad (7)$$

Another reactivity descriptor that enables the quantification of a compound's electrophilic nature on a relative scale is the electrophilic character (ω). We used Eq. (8) to determine the extent of the reduction in maximum energy resulting from the transfer of electrons from the donor to the acceptor. Furthermore, the electrophilicity index of a chemical species has been defined by Parr et al. as the result of dividing the square of electronegativity by the chemical hardness [36].

$$\omega = \frac{\mu^2}{2} \times S = \frac{\mu^2}{2\eta} \quad (8)$$

Recently, Gázquez *et al.* [31] have determined the electroaccepting (Eq. (9)), ω^+, and electrodonating (Eq. (10)), ω^-, powers as:

$$\omega^+ = \frac{EA^2}{2(IE-EA)} \quad (9)$$

$$\omega^- = \frac{IE^2}{2(IE-A\ )} \quad (10)$$

Where ω^+ indicates the ability of the molecular system to accept charges and ω^- represents the ability to give charges. We note that a higher ω^+ value indicates a system's ability to take charge (accept charge); in contrast, a system with a lower ω^+ value is a better electron donor.

We have also used the following equation (Eq. (11)) to compute the highest number of electrons that an electrophile can obtain using the quantum chemical approach [36,37]:

$$\Delta Nmax = \frac{-\mu}{\eta} \quad (11)$$

Equation (12), which is represented by the term flowing, gives us the global electrophilicity gap Δω of the reagents:

$$\Delta\omega = \omega_{electophil} - \omega_{nuclephile} \quad (12)$$

When dealing with closed-shell organic molecules, it is possible to use an empirical nucleophilic index N that relies on HOMO energies [38,39], E_{HOMO} calculated using the Kohn-Sham scheme [40], and defined as follows (Eq. (13)):

$$N = E_{HOMO\ (Nucleophile)} - E_{HOMO\ (TCE)} \quad (13)$$

It is important to note that the nucleophilicity scale references tetracyanoethylene (TCE). Based on DFT/B3LYP/631G(d) estimations, the $E_{HOMO(TCE)}$ is approximately -9.1623 eV.

RESULTS AND DISCUSSION

Optimization of Molecules

Figure 3 displays the achieved optimized molecules achieved using the B3LYP functional with the 6-31G(d) basis set. The atomic numbering of the most stable geometries is also provided.

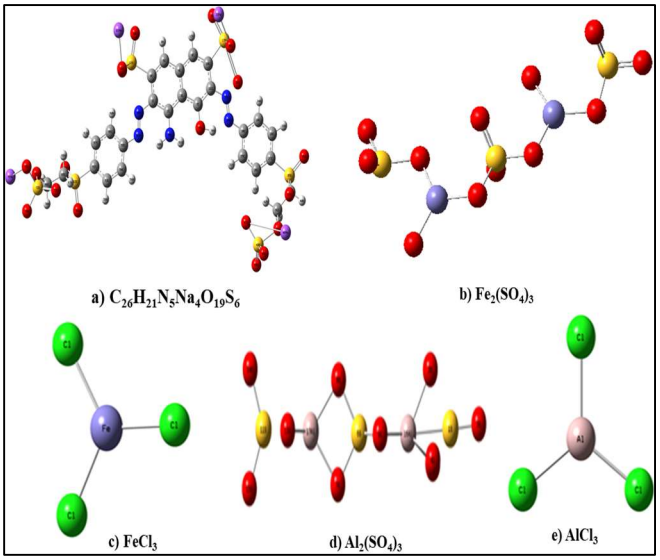

Fig. 3. Optimized molecules of RB5 dye (a) and the coagulants $Fe_2(SO_4)_3$ (b), $FeCl_3$ (c) $Al_2(SO_4)_3$ (d), and $AlCl_3$) (e) using the DFT-B3LYP/6-31G(d) basis set.

Analysis of Global Molecular Reactivity

The global chemical reactivity descriptors were calculated individually for the RB5 dye and the coagulants $Fe_2(SO_4)_3$, $FeCl_3$, $Al_2(SO_4)_3$, and $AlCl_3$. The global descriptors, namely, the energy gap, the electronic chemical potential (μ), the dipole moment, the chemical hardness (η), the electrophilicity (ω), and the nucleophilicity (N) at the ground state (GS) of the reagent's reactions, are analyzed in this work. These descriptors were employed in order to study the interaction mechanism between RB5 dye and these various coagulants and to predict their reactivity.

Energy Gap

Table 3 and Fig. 4 summarize the results of calculating the energy gap (ΔE_{gap}) for various reagents. The computed HOMO energy values for the RB5 dye and the coagulants $Fe_2(SO_4)_3$, $FeCl_3$, $Al_2(SO_4)_3$, and $AlCl_3$ are -5.916, -7.976, -8.528, -9.254, and -9.263 eV for HOMO, respectively. In this case, RB5 dye has a higher HOMO energy (-5.916 eV) which corresponds to a more reactive molecule in electrophile reactions, whereas $AlCl_3$ has a lower HOMO energy (-9.263 eV) which corresponds to a less reactive molecule in nucleophile reactions. The reaction occurs because there is a high likelihood of interaction between the HOMO of the RB5 molecule and the LUMO of $Fe_2(SO_4)_3$. Hence, electrons can transit freely from the HOMO of RB5 dye into the LUMO of $Fe_2(SO_4)_3$, leading to the higher coagulation-flocculation capacity of the dye molecules compared to other reagents.

Thus, as noted in Table 3 and Fig. 4, the LUMO energy values for RB5 dye, $Fe_2(SO_4)_3$, $FeCl_3$, $Al_2(SO_4)_3$, and $AlCl_3$ molecules are -3.600, -6.081, -6.231, -6.475, and -3.078 eV, respectively. The negative magnitude of E_{HOMO} and E_{LUMO} has indicated that $AlCl_3$ is more stable than other studied molecules. According to the E_{gap} computation, which analyzes the chemical reactivity and kinetic stability of a molecule. The reactants can be ranked based on their energy gap as follows: Energy gap $Fe_2(SO_4)_3$ < $FeCl_3$ < RB5 < $Al_2(S0_4)_3$ < $AlCl_3$. This ranking shows that the molecule $Fe_2(SO_4)_3$ has the lowest energy gap difference (ΔE_{gap} = 1.895 eV). Due to its polarizability, RB5 is commonly linked with high reactivity and low kinetic stability, making it a "soft" molecule. RB5 tends to exchange electron density with $Fe_2(SO_4)_3$, indicating its high electro-acceptance power ($\omega^+(Fe_2(SO_4)_3)$ = 9.754 eV) (Table 5).

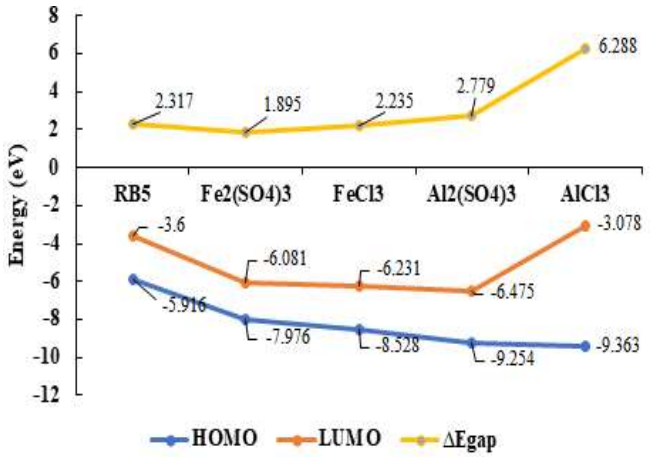

Fig. 4. Graph of Energies HOMO, LUMO, ΔEgap descriptors for the RB5 dye and the coagulants $Fe_2(SO_4)_3$, $FeCl_3$, $Al_2(SO_4)_3$, and $AlCl_3$.

Table 3. Energies HOMO, LUMO, $\Delta E_{gap,}$ of the RB5 Dye and the Coagulants $Fe_2(SO_4)_3$, $FeCl_3$, $Al_2(SO_4)_3$, and $AlCl_3$ Using the DFT-B3LYP/6-31G(d) Basis Set

Reagents	E(RB3LYP) (a.u)	HOMO (eV)	LUMO (eV)	ΔE_{gap} (eV)
RB5	-5742.89	-5.916	-3.600	2.317
$Fe_2(SO_4)_3$	-4623.51	-7.976	-6.081	1.895
$FeCl_3$	-2644.16	-8.528	-6.231	2.235
$Al_2(SO_4)_3$	-2581.27	-9.254	-6.475	2.779
$AlCl_3$	-1623.14	-9.363	-3.078	6.288

a.u: atom unit; eV: electron volt.

Ionization Energy (IE) and Electron Affinity (EA)

Figure 5 provides the IE and EA values calculated through the difference method. As per the results, RB5 displays lower ionization potential values, confirming its electron donor character compared to other molecules. $Fe_2(SO_4)_3$ molecule exhibits the highest EA value, confirming its electron acceptor ability. On the other hand, $AlCl_3$ is found to be more stable.

Dipole Moment (μ)

The dipole moment (μ) is an important electrical

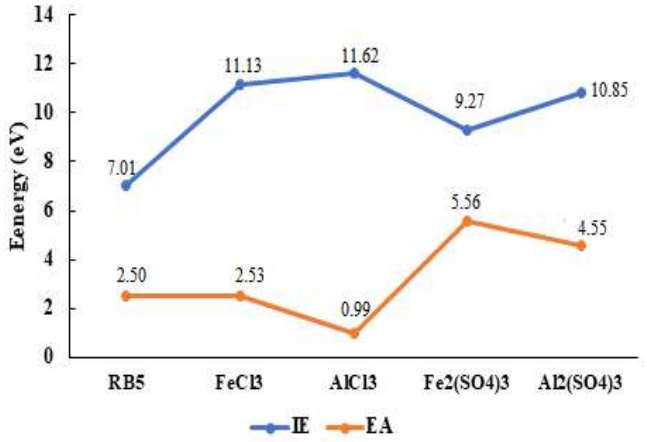

Fig. 5. Graph of Ionization Energy (IE) and Electron Affinity (EA) descriptors the RB5 dye and the coagulants $Fe_2(SO_4)_3$, $FeCl_3$, $Al_2(SO_4)_3$, and $AlCl_3$ using the DFT-B3LYP/6-31G(d) basis set.

Table 4. Value of the Dipole Moment of the RB5 Dye and the Coagulants $Fe_2(SO_4)_3$, $FeCl_3$, $Al_2(SO_4)_3$, and $AlCl_3$ Using the DFT-B3LYP/6-31G (d) Basis Set

Reagents	Dipole moment (in Debye)
RB5	16.8480
$Fe_2(SO_4)_3$	2.5146
$FeCl_3$	0.3117
$Al_2(SO_4)_3$	3.1754
$AlCl_3$	0.0000

parameter that reveals the polarity of the entire molecule. Table 4 displays the dipole moment values of the RB5 dye and the coagulants $Fe_2(SO_4)_3$, $FeCl_3$, $Al_2(SO_4)_3$, and $AlCl_3$ using the DFT-B3LYP/6-31G(d) basis set.

Chemical reactivity is most likely due to the strong molecular polarity. According to the literature [41], reagents with significant dipole moments are more reactive, resulting in a considerable increase in elimination efficiency. When compared to other molecules, the high dipole moment value of RB5 dye (μ =16.8480 Debye) likely improves coagulation between the dye and the reagent $Fe_2(SO_4)_3$ (μ = 2.5146 Debye).

Hardness (η) and Softness (S)

Figure 6 shows the studied reagent's global hardness and softness data. Understanding a molecule's stability and reactivity requires knowledge of its global hardness (η) and softness (S), which are the key characteristics. Chemical hardness is a term for assessing chemical reactivity and defining a system's charge transfer resistance. The lower the values, the more likely an electron transfer will occur in the system. A rigid molecule typically has a wider energy gap, while a soft molecule typically has a narrower one [41]. It is important to remember that electronic systems with complex molecules are less prone to reactions, whereas systems with softer molecules are more likely to react. A molecule with a low chemical hardness and a high softness value tends to be eliminated at a higher rate.

From the data presented in Fig. 6, it has been observed that the $Fe_2(SO_4)_3$ molecule has the lowest hardness (η = 0.95 eV) and the highest softness (S = 1.06 eV), which explains their higher reactivity with RB5 compared with the other molecules, particularly $AlCl_3$. The latter has the highest hardness value (η = 3.14 eV) and the lowest softness value (S = 0.32 eV). It is the compound that is the most resistant to electron transfer and therefore the most stable compound. Based on the hardness criterion, the ranking of the reagents is as follows: (η, S) $Fe_2(SO_4)_3$ < (η, S) $FeCl_3$ < (η, S) RB5 < $Al_2(SO_4)_3$ < (η, S) $AlCl_3$.

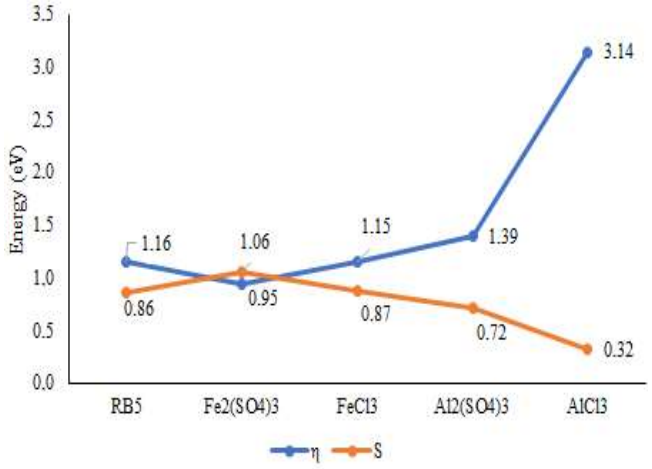

Fig. 6. Graph of global hardness (η) and softness (S) index of the RB5 dye and the coagulants $Fe_2(SO_4)_3$, $FeCl_3$, $Al_2(SO_4)_3$, and $AlCl_3$ using the DFT-B3LYP/6-31G(d) basis set.

Global Electrophilicity (ω) and the Nucleophilicity Index (N)

It is simple to anticipate the electrophilic-nucleophilic interactions in the transition state structure by analyzing the electrophilicity/nucleophilicity index that the CDFT provides for the reagents at the ground state [37]. Table 5 and Fig. 7 show that the $Fe_2(SO_4)_3$ molecule has the highest and most intense electrophilicity index (ω = 26.063 eV) compared to the RB5 dye (ω = 9.776 eV) and $AlCl_3$ (ω = 6.156 eV).

Based on these data, it appears that ω $Fe_2(SO_4)_3$ has a higher electrophilicity compared to ω $FeCl_3$, ω$Al_2(SO_4)_3$, ω(RB5), and ω($AlCl_3$). The $Fe_2(SO_4)_3$ molecule has a greater proton count and a deficiency of electrons, making it a more efficient acceptor than $AlCl_3$, which lacks electrons. Analyzing the electroaccepting, ω^+, and electrodonating, ω^-, indices given in Table 5 reveals a similar trend, $\omega^+(Fe_2(SO_4)_3) > \omega^+(FeCl_3) > \omega^+(Al_2(SO_4)_3) > \omega^+(RB5) > \omega^+(AlCl_3)$. As a result, $Fe_2(SO_4)_3$ tends to acquire additional electronic charge and will react quickly and easily with the RB5 dye serving as a nucleophilic donor, followed by $FeCl_3$. However, the energy gap of $AlCl_3$ is higher (6.288 eV). Thus, this molecule is hard $\eta(AlCl_3)$ = 3.143 (eV) > η(RB5) = 1.158 (eV) > $\eta(FeCl_3)$ = 1.148 (eV), presenting an electrophilicity ω index of 6.156 eV being classified as a weak electrophile. Based on the information in Table 5, the nucleophilicity index of RB5 (N = 3.247 eV) is greater than that of the $Fe_2(SO_4)_3$ reagent (N = 1.186 eV). This implies that in this reaction, the RB5 dye is considered a nucleophile while $Fe_2(SO_4)_3$ or the other molecules are electrophiles.

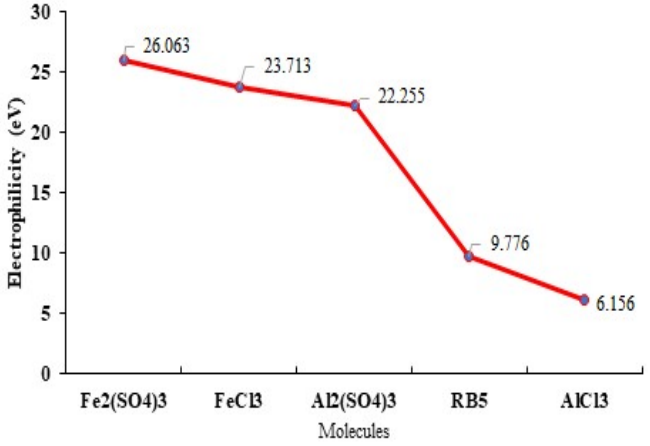

Fig. 7. Graph of electrophilicity index of the RB5 dye and the coagulants $Fe_2(SO_4)_3$, $FeCl_3$, $Al_2(SO_4)_3$, and $AlCl_3$ using the DFT-B3LYP/6-31G(d) basis set.

Chemical Electron Potential (μ) and Electronegativity (χ)

The data presented in Fig. 8 shows that the chemical potentials are the opposite of the electronegativities. This prompts us to consider one of one of these two descriptors. Additionally, the RB5 dye has the lowest electronegativity value (χ = 4.758 eV) compared to the other reactants. This is due to its larger atomic size, which results in a lower electronegativity value (the molecular weight is 991.82 g mol^{-1}).

The RB5 dye has a higher chemical potential μ of (μ = -4.758 eV) than that of $Fe_2(SO_4)_3$ (μ = -7.028 eV) or

Table 5. Value of the Global Electrophilicity (ω), Electroaccepting (ω+) Electrodonating (ω-), Δω, the Nucleophilicity Index N, and ΔN_{max} the RB5 Dye and the Coagulants $Fe_2(SO_4)_3$, $FeCl_3$, $Al_2(SO_4)_3$, and $AlCl_3$ Using the DFT-B3LYP/6-31G (d) Basis Set

Reagents	ω (eV)	ω+ (eV)	ω- (eV)	Δω (eV)	N (eV)	ΔN_{max} (eV)
RB5	9.776	2.798	2.094	-	3.247	4.109
$Fe_2(SO_4)_3$	26.063	9.754	2.426	16.287	1.186	7.417
$FeCl_3$	23.713	8.454	2.672	13.937	0.634	6.427
$Al_2(SO_4)_3$	22.255	7.543	2.986	12.480	-	5.660
$AlCl_3$	6.156	0.753	4.715	-	-	1.979

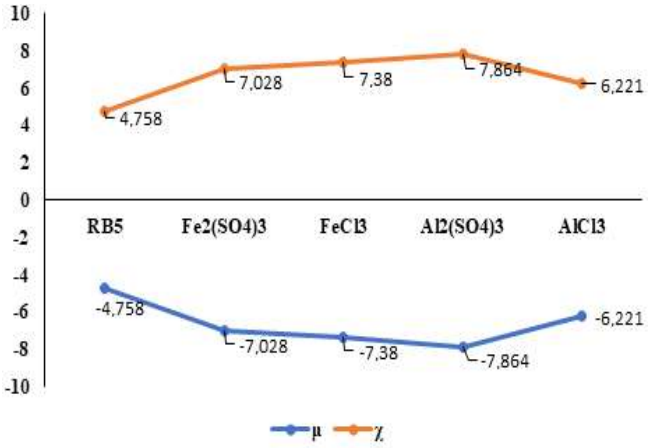

Fig. 8. Graph of chemical potential (μ) and electronegativity (χ) index of the RB5 dye and the coagulants $Fe_2(SO_4)_3$, $FeCl_3$, $Al_2(SO_4)_3$, and $AlCl_3$ using the DFT-B3LYP/6-31G(d) basis set.

$AlCl_3$ (μ = -6.221 eV) or $FeCl_3$ (μ = -7.380 eV). This result indicates that the RB5 dye has a nucleophilic character, whereas $Fe_2(SO_4)_3$ or the other reagents have an electrophilic character (the reagent RB5 will act as an electron donor, and other reagents will act as electron acceptors). The electron transfer from RB5 dye to $Fe_2(SO_4)_3$ or $FeCl_3$ is straightforward, resulting in system stabilization. The ranking of the chemical electron potential of the reagents is as follows: μ(RB5)> μ ($AlCl_3$) > μ ($Fe_2(SO_4)_3$) > μ ($FeCl_3$) > μ ($Al_2(S0_4)_3$).

The results of the calculation of the chemical potential (μ) and electronegativity are in agreement with those found by the two theoretical methods: HOMO/LUMO deviations and electrophilic indices (ω). We conclude, therefore, that the compound RB5 dye acts as a nucleophile (electron donor). However, the compound $Fe_2(SO_4)_3$ acts as an electrophile (electron acceptor).

Analysis of Frontier Molecular Orbitals

One of the better theories and useful tools for analyzing and explaining a molecule's chemical stability is the frontiers molecular orbitals (FMOs) theory, which involves HOMO and LUMO orbitals. When examining a molecule's reactivity, the FMO concept analyzes the interactions between the molecular orbitals of the reactants. This approach focuses solely on the most crucial interactions. However, it provides valuable insights [42,43]. Additionally, E_{HOMO} and E_{LUMO} offer details on energy distribution, energetic activity, and how molecular entities interact. Understanding the energies of HOMO and LUMO is crucial to gaining insights into energy distribution, energetic activity, and molecular interactions.

To determine the nucleophilic donor or electrophilic acceptor character of the RB5 dye and the coagulants $Fe_2(SO_4)_3$, $FeCl_3$, $Al_2(SO_4)_3$, and $AlCl_3$, we have computed the energy gaps between their HOMO and LUMO. Figure 9a and Figure 9b summarize the findings of this research. The results show that the gap $|E_{HOMO\ (RB5)} - E_{LUMO\ (Fe2(SO4)3}| = 0.1649$ eV and $|E_{HOMO\ (Fe2(SO4)3} - E_{LUMO\ (RB5)}| = 4.3758$ eV was smaller than the gap of the other possible combinations, indicating that reactive Black-5 dye behaves as an electron donor and $Fe_2(SO_4)_3$ is an electron acceptor.

Using the criterion of the energy gap of the reactants in absolute value, the ranking of the reactants is as follows: $|E_{HOMO}$ (RB5)-E_{LUMO} ($Al_2(SO_4)_3$| < $|E_{HOMO}$ (RB5)-E_{LUMO} ($FeCl_3$)| < $|E_{HOMO}$ (RB5)-E_{LUMO} ($Al_2(SO_4)_3$| < $|E_{HOMO}$ (RB5)-E_{LUMO} ($AlCl_3$| and $|E_{HOMO}$ ($Fe_2(SO_4)_3$-E_{LUMO} (RB5)| < $|E_{HOMO}$ ($FeCl_3$)-E_{LUMO} (RB5)| < $|E_{HOMO}$ ($Al_2(SO_4)_3$-E_{LUMO} (RB5)| < $|E_{HOMO}$ ($AlCl_3$)-E_{LUMO} (RB5)|. Based on the data obtained, the Reactive Black 5 dye behaves as a nucleophilic donor. While the ferric sulphate operates as an electrophilic acceptor. The preferential reaction of the RB5 dye with the coagulant $Fe_2(SO_4)_3$ over other reagents is attributed to this behavior.

Based on the diagrams in Figs. 9a and 9b, we conclude that the HOMO orbital is strongly condensed on and around the C1 to C11 benzene ring and part of the other C52 to C57 benzene ring. In contrast, the LUMO is condensed on the C1 to C11 benzene ring, N23, N24, and C25 to C30 benzene ring. Based on this data, the nucleophilic attack is mainly on and around these benzene rings and nitrogen regions. Analysis of the Fukui index or Parr function can be exploited to identify which atoms the nucleophilic attack will occur on.

Molecular Electrostatic Potentials

The molecular electrostatic potentials (MEPs) model reflects a molecule's reactivity and informs us how electric charge is distributed among a molecule. In this case, MEP determines whether the areas are nucleophilic or electrophilic based on their color reactivity [44,45]. The neutral MEPs of the RB5 dye and the coagulants $Fe_2(SO_4)_3$, $FeCl_3$, $Al_2(SO_4)_3$,

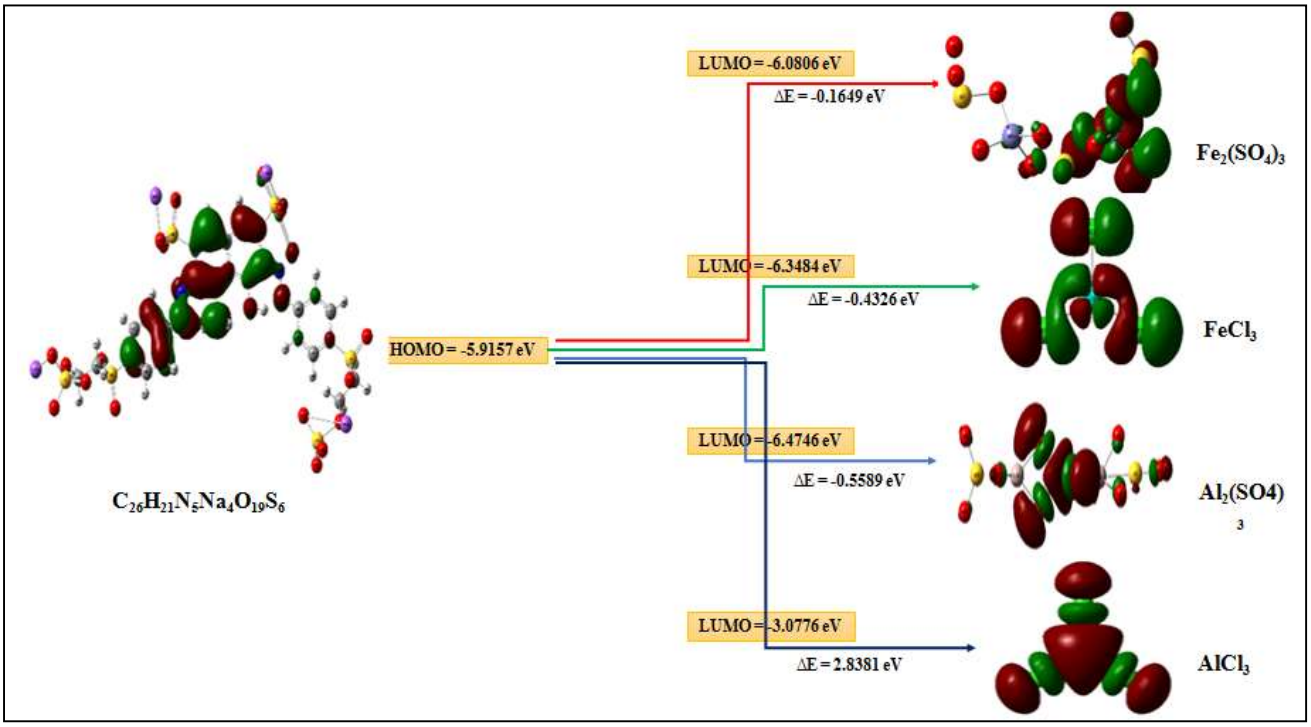

Fig. 9a. Distribution of FMOs for the RB5 dye and the coagulants $Fe_2(SO_4)_3$, $FeCl_3$, $Al_2(SO_4)_3$, and $AlCl_3$ using the DFT-B3LYP/6-31G(d) basis set.

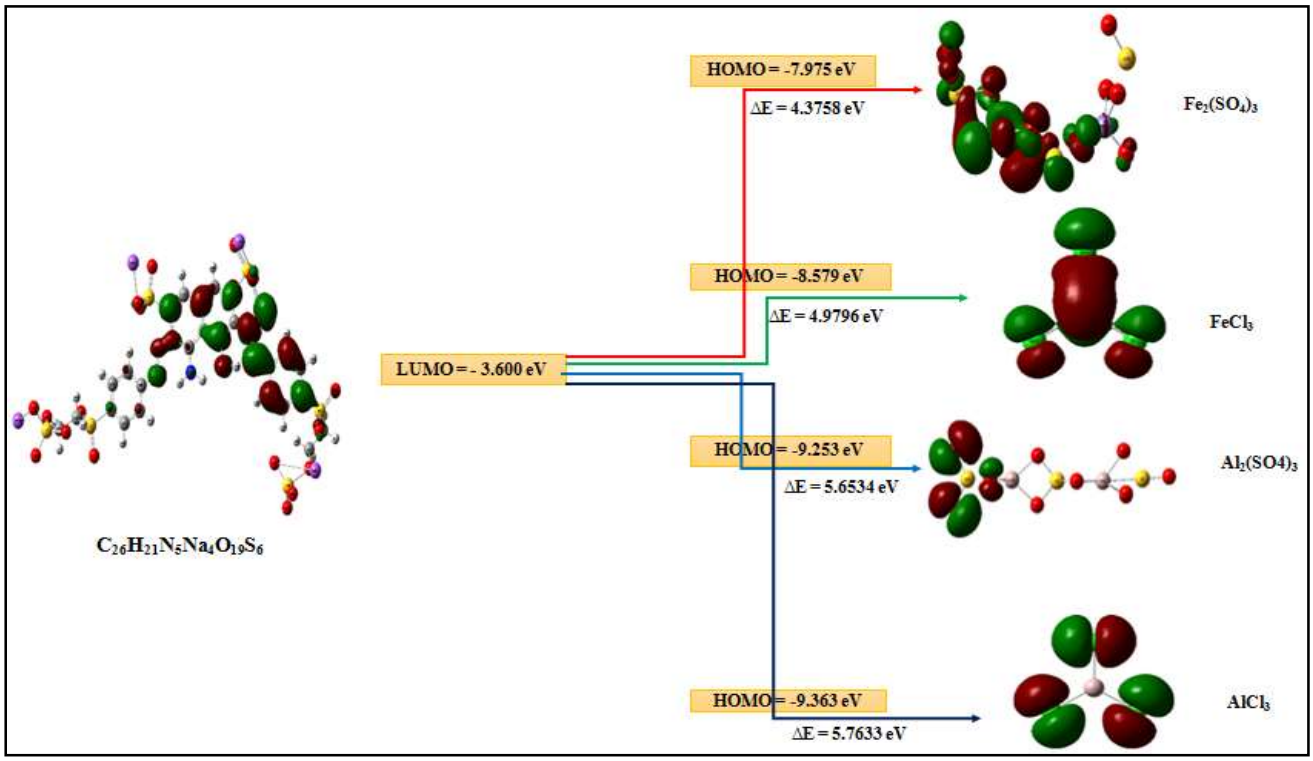

Fig. 9b. The energy gap between nucleophilic LUMO and electrophilic HOMO calculated using the DFT-B3LYP/6-31G(d) basis set for the RB5 dye and the coagulants $Fe_2(SO_4)_3$, $FeCl_3$, $Al_2(SO_4)_3$, and $AlCl_3$.

and $AlCl_3$ have been calculated and plotted based on the optimized geometry.

In Fig. 10, a range of colors depicts the electrostatic potential on the molecule's surface. This map is neatly color-coded in line with the visible spectrum. The orange-red areas represent the negative charge part of the molecule (electrophilic reactivity). The blue region represents the positively charged region (nucleophilic reactivity). The

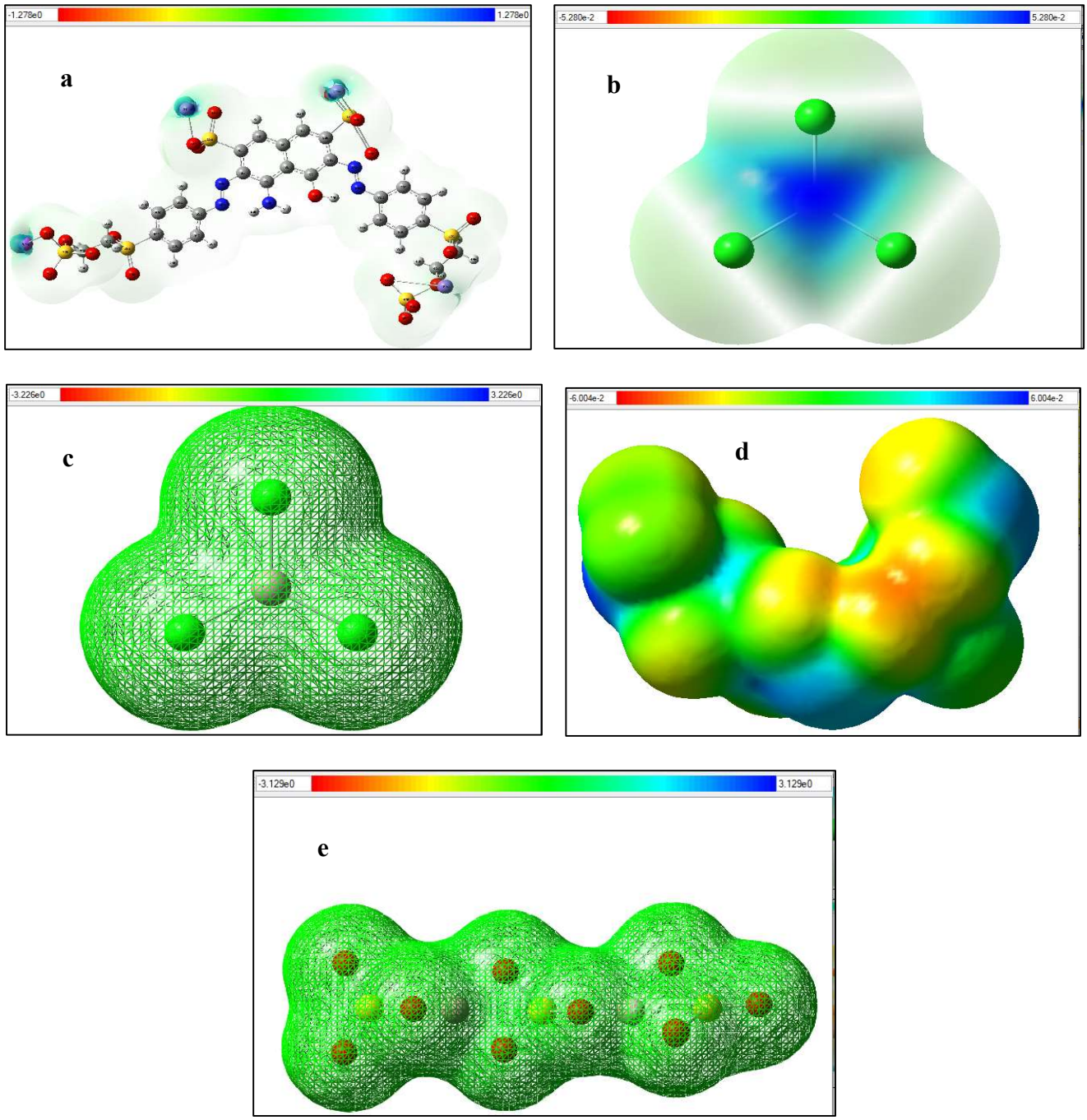

Fig. 10. Molecular electrostatic potentials maps for the Neutral RB5 (a), neutral $FeCl_3$ (b), neutral $AlCl_3$ (c), neutral $Fe_2(SO_4)_3$ (d), and neutral $Al_2(SO_4)_3$ (e).

succession is as follows: red (strong negative electrostatic potential (EP)) > orange > yellow > green (moderately positive EP) > blue (strong positive EP). For the studied molecules, the color code of the MEP diagram ranges from -1.278 atomic units (dark red) to 1.278 atomic units (dark blue) for neutral RB5 (a), -5.280 10^{-2} atom units (dark red), and 5.280 10^{-2} atom units (dark blue) for neutral $FeCl_3$ (b), -3.226 atom units (dark red) and 3.226 atom units (dark blue) for neutral $AlCl_3$ (c), -6.004 10^{-2} atom units (dark red) and 6.004 10^{-2} atom units (dark blue) for neutral $Fe_2(SO_4)_3$ (d), and -3.129 atom units (dark red) and 3.129 atom units (dark blue) for neutral $Al_2(SO_4)_3$ (e).

From the electrostatic potential distribution, the deep dark blue region (more protons and a deficiency of electrons) is located around the sulfur atoms of the neutral $Fe_2(SO_4)_3$ molecule (d), representing their electrophilic nature (nucleophilic attack locale). It reveals that the $Fe_2(SO_4)_3$ molecule is a more electrophilic acceptor; the neutral $FeCl_3$ molecule (b) presents similar behavior. These regions would be the ideal locations for its reactivity to the RB5 dye (as a nucleophilic donor). Multiple C=O double bonds and hydroxyl groups characterize the RB5 molecule (a). Based on the map presented in Fig. 10a, it is evident that the majority of areas surrounding the benzene ring exhibit a slightly negative value, while the regions surrounding each C–H, N–H, N=N, and O–H bond present positive ESP. Consequently, the $Fe_2(SO_4)_3$ or $FeCl_3$ coagulant can effectively eliminate it due to the molecule's strong electrostatic force (electronegativity (χ) $Fe_2(SO_4)_3$ and $FeCl_3$ > electronegativity (χ) index of RB5 dye). Furthermore, the MEP diagram confirms the stability of the neutral $AlCl_3$ and $Al_2(SO_4)_3$ (green: moderately positive (EP)).

Analysis of the Density of the State Spectrum

Figure 11 shows the Density of State graphs (DOS) at B3LYP6-31G(d) for the studied molecules. These graphs display the HOMO and LUMO, represented by green and red lines, respectively. The energy gap between the HOMO and LUMO levels for all studied elements is represented by the area between the green and red lines.

The DOS diagram illustrates the energies available for transitions, such as thermal excitation. An electron in a valence band (an occupied band, someplace below the Fermi energy) can absorb energy and momentum and move into a conduction band (an unoccupied band, someplace above the Fermi energy), where the energy difference between the final and initial states is identical to the energy absorbed. The probability of this taking place is linked to the density of states at the initial and final energies.

Moreover, the analysis of the DOS diagrams shows a uniform distribution of HOMO and LUMO for all the elements studied (Fig. 11). The density of HOMO in all the compounds studied can be observed from the density of state diagrams. The distributions of all the compounds show that the contributing elements have a higher LUMO density than the central element. The DOS plots frequently verify that the density shift from the source regions to the central region occurs in all compounds.

Analysis of Local Molecular Reactivity Fukui Function

In this framework, our compound's most favorable electrophilic and nucleophilic centers are evaluated using a local chemical reactivity analysis based on the Fukui function. We examined the local molecular reactivity to identify the atoms or molecular locations targeted by the chemicals and to understand why specific reagents are more effective than others. The static indices of local nucleophilicity N_k [46] and local electrophilicity ω_k [47] are accurate descriptors for forecasting the most favorable electrophilic-nucleophilic interaction for the chemical production of a chemical bond between two atoms, following the Domingo polar model [17]. It occurs between the most nucleophilic site of the nucleophilic molecule, shown by the most substantial value of N_k, and the most electrophilic site of the electrophilic molecule, which is indicated by the most considerable value of ω_k.

We have used the Fukui function f(r) (Eqs. (16)-(19)), which we acquired by examining the Mulliken atomic charge density (MACD), to treat the molecules' anionic and cationic radicals.

$$\omega_k = \omega f_k^+ \tag{16}$$

$$N_k = N f_k^- \tag{17}$$

Where one has used

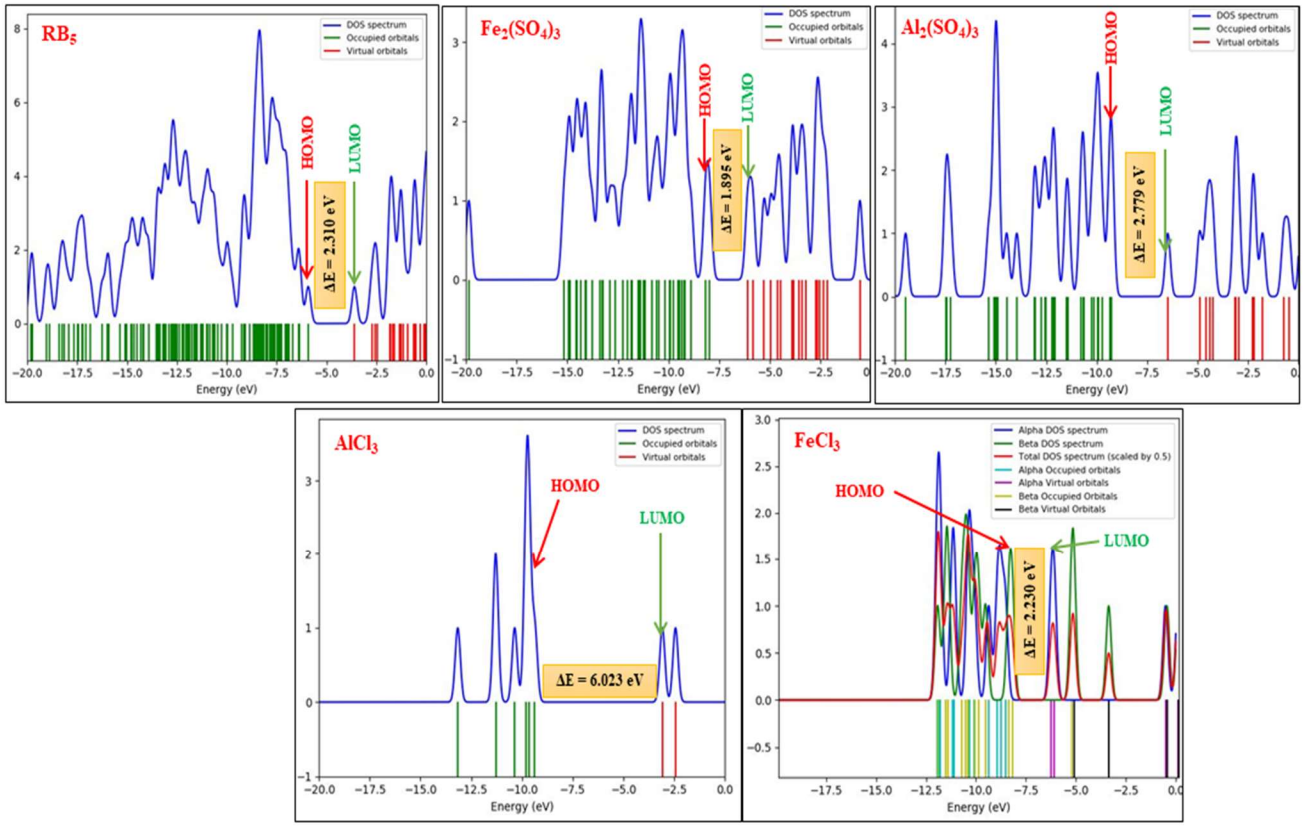

Fig. 11. The designed compound density of state graphs at B3LYP6-31G(d).

$$f_k^+ = \left(q_k(N+1) - q_k(N)\right) \quad \text{for a nucleophilic attack} \tag{18}$$

$$f_k^- = \left(q_k(N) - q_k(N-1)\right) \quad \text{for an electrophilic attack} \tag{19}$$

With $q_k(N)$ represents the electron population of atom K in the neutral molecule, $q_k(N+1)$ representing the electron population of atom K in the anionic molecule, and $q_k(N-1)$ representing the electron population of atom K in the cationic molecule (ω = 9.776 eV) and (N = 3.247 eV).

The sites with the highest values (most reactive and favorable sites) of the local electrophilic (ω_k) and local nucleophilic (N_k) are listed in Table 6. We discover that the nitrogen (-N79) atom has the highest Fukui value (ω_k = 0.519 eV) when compared to other atoms, followed by the benzene ring region, particularly in-C5-H9 (ω_k = 0.449 eV) and $-C1$ (ω_k = 0.365 eV) and -Na21 (ω_k = 0.363 eV), -Na22 (ω_k = 0.364 eV) and -N51 (ω_k = 0.302 eV) atoms. They are the most preferred reaction sites for nucleophilic attacks.

Parr Function

Based on the analyze the Mulliken Atomic Spin Density (MASD) [48], the Parr function P(r) was used to examine the anionic and cationic radicals of the RB5 dye. The neutral system has two functions: the nucleophilic Parr function and the electrophilic Parr function [49]. On the other hand, our Parr function research provided the use of the local nucleophilicity N_k and electrophilicity ω_k [17] indices to identify the atoms or locations active in the dye that are participating in the attack action. Table 7 gives the estimated P(r) indices for the Parr function. The following equations (Eqs. (20)-(23)) [48] yield these functions:

$$\omega_k = \omega P_k^+ \tag{20}$$

Table 6. Fukui Ffunction, Local Electrophilicity (ω_k), and Local Nucleophilicity (N_k) Calculated in eV Using the DFT-B3LYP/6-31G(d) Basis Set

Dye	Mulliken atomic charges				Fukui functions		ω	N	ω_k	N_k
	Atoms	q(N+1)	qN0	q(N-1)	f_k^+	f_k^-				
RB5	C1	0.263	0.225	0.219	0.037	0.007	9.776	3.247	0.365	0.022
	C5	-0.119	-0.165	-0.168	0.046	0.003	9.776	3.247	0.449	0.009
	H9	0.252	0.216	0.197	0.036	0.019	9.776	3.247	0.351	0.062
	C11	0.433	0.412	0.423	0.021	-0.011	9.776	3.247	0.207	-0.037
	H12	0.242	0.218	0.197	0.023	0.022	9.776	3.247	0.227	0.070
	S17	1.101	1.072	1.056	0.029	0.016	9.776	3.247	0.280	0.051
	O19	-0.316	-0.339	-0.409	0.023	0.070	9.776	3.247	0.222	0.228
	Na21	0.749	0.712	0.680	0.037	0.032	9.776	3.247	0.363	0.103
	Na22	0.683	0.646	0.596	0.037	0.049	9.776	3.247	0.364	0.160
	N51	-0.349	-0.380	-0.401	0.031	0.021	9.776	3.247	0.302	0.068
	H58	0.229	0.202	0.187	0.027	0.015	9.776	3.247	0.260	0.049
	H59	0.172	0.149	0.139	0.023	0.010	9.776	3.247	0.221	0.034
	H61	0.220	0.194	0.179	0.026	0.015	9.776	3.247	0.255	0.049
	O63	-0.586	-0.606	-0.619	0.021	0.013	9.776	3.247	0.204	0.041
	O64	-0.574	-0.595	-0.607	0.021	0.013	9.776	3.247	0.205	0.041
	N79	-0.733	-0.786	-0.789	0.053	0.003	9.776	3.247	0.519	0.010
	H80	0.394	0.372	0.361	0.022	0.012	9.776	3.247	0.215	0.038
	H81	0.401	0.374	0.369	0.027	0.005	9.776	3.247	0.265	0.017

Table 7. Theoretical Prediction of Reactive Sites Using Parr Function for RB5 Dye (in eV)

Dye	N° of atom	Atom	P_k^-	P_k^+	ω	N	ω_k	N_k
RB5	1	C	0.273	-0.020	9.776	3.247	2.671	-0.066
	4	C	-0.111	0.139	9.776	3.247	-1.085	0.453
	5	C	0.286	-0.072	9.776	3.247	2.797	-0.235
	6	C	-0.145	0.112	9.776	3.247	-1.419	0.362
	7	C	-0.005	0.066	9.776	3.247	-0.051	0.213
	8	C	0.137	-0.077	9.776	3.247	1.340	-0.251
	10	C	-0.025	0.123	9.776	3.247	-0.247	0.399
	11	C	0.103	-0.084	9.776	3.247	1.011	-0.272
	19	O	-0.039	0.219	9.776	3.247	-0.383	0.711
	23	N	-0.029	0.217	9.776	3.247	-0.286	0.705
	24	N	0.071	0.061	9.776	3.247	0.695	0.197
	25	C	0.031	0.052	9.776	3.247	0.298	0.168
	27	C	0.035	0.080	9.776	3.247	0.340	0.259
	29	C	0.031	0.057	9.776	3.247	0.304	0.185
	51	N	0.181	0.059	9.776	3.247	1.769	0.190
	52	C	0.116	0.023	9.776	3.247	1.137	0.076
	54	C	0.086	0.018	9.776	3.247	0.843	0.059
	56	C	0.087	0.022	9.776	3.247	0.848	0.072
	79	N	0.201	-0.019	9.776	3.247	1.968	-0.063

$$N_k = NP_k^- \quad (21)$$

Where ω and N are the electrophilicity and nucleophilicity index, respectively (Table 4).

$$P_k^+ = \rho_s^{rc}(r) \text{ for electrophilic attacks} \quad (22)$$

$$P_k^- = \rho_s^{ra}(r) \text{ for nucleophilic attacks} \quad (23)$$

Where $\rho_s^{rc}(r)$ is the ASD of the radical cation, and $\rho_s^{ra}(r)$ is the ASD of the radical anion.

The calculated Parr functions P_k^+ and P_k^- has been calculated and listed in Table 7.

Table 7 lists the computed Parr functions, including the cationic system's local nucleophilicP_k^- Parr functions, the anionic system's electrophilic P_k^+ Parr functions, and the local electrophilicity and nucleophilicity of the RB5 dye are being studied.

The Mulliken ASD of the radical anion and radical cation were examined to determine their electrophilic and nucleophilic properties. The properties of these materials were analyzed through the computation of indices using the restricted B3LYP-6-31G(d) methodology for radical species. Additionally, single-point energy computations were performed on the optimized neutral geometries.

Table 7 demonstrates that the most vulnerable sites for a nucleophilic attack which have the highest values of ω_k, are on the benzene rings (C5-9H $\omega_k = 2.797$ eV, C1-50N $\omega_k = 2.671$ eV), the nitrogen region (-N79-80H-81H $\omega_k = 1.968$eV, -N51 = N50- $\omega_k = 1.769$ eV) and sulfur (C52-62S $\omega_k = 1.137$ eV). Similarly, this calculation showed that the most reactive site in the case of a nucleophilic attack of the RB5 dye is in the C5-9H bonding region (ω_k = 2.797 eV). Also, the most vulnerable locations to electrophilic attacks on RB5, which have the highest values of N_k are the sulfur region (O19-17S$N_k = 0.711$ eV) and Nitrogen region (-N23=N24- $N_k = 0.705$ eV); with (O19-17S $N_k = 0.711$ eV) is the most reactive site in the case of an electrophilic attack.

EXPERIMENTAL STUDY OF REACTIVE BLACK-5 DYE REMOVING

Experimental Methodology

The present experimental study aims to validate the theoretical results obtained using the DFT-B3LYP/6-31G(d) basis set by testing these four coagulants under optimal conditions that achieve the highest COD reduction rate. The detailed results of this experimental study will be the subject of our next research article. This study performed coagulation experiments using the Jar Test, an apparatus with six bakers' sizes of 1,000 ml. The effluent containing RB5 dye and coagulants was prepared previously and introduced into bakers with different doses of coagulants under controlled and reproducible conditions (Table 8). The coagulants used are ferric sulphate ($Fe_2(SO_4)_3$), ferric chloride ($FeCl_3$), aluminium sulphate ($Al_2(SO_4)_3$ and aluminium chloride ($AlCl_3$). The characteristics of these coagulants are listed in Table 2. To adjust the pH, 0.1 M HCl or NaOH solutions were added.

The % removal COD was calculated using Eq. (24):

$$\%\text{Removal COD} = \frac{(C_i - C_f)}{C_i} * 100 \quad (24)$$

Where C_i and C_f are the initial and final concentrations of the COD parameter.

Table 8. Range of Essential Parameters Obtained from the Literature

Parameters	Range	Ref.	The range used in the present work
Speed of rapid mixing (rpm)	100-250	[14] [50]	150
Duration of rapid mixing (min)	1-5	[14] [50]	1
Speed of slow mixing (rpm)	30-60	[14]	30
Duration of slow mixing (min)	10-55	[14]	15
Settling time (min)	30-120	[14]	30

Effect of Coagulant Dosage on %COD Removal

An experimental investigation was conducted to evaluate the effectiveness of the studied coagulants on COD removal. To achieve the best results, the ideal pH level was established for each coagulant based on an initial COD concentration of 500 mg l^{-1}. The presented values are the result of our study on the impact of various parameters on eliminating the RB5 dye. This topic will be further addressed in the upcoming articles. We investigated the coagulation of RB5 dye by altering the quantity of coagulant within a specific range (5, 50, 100, 150, 200, and 250 mg l^{-1}); the optimal dose of coagulant was 200 mg/L obtained for each coagulant. Figure 12 summarizes the optimal operating conditions that resulted in high COD removal for the four coagulants.

The coagulation process is influenced by the pH level of the medium. In acidic medium, the presence of $Fe_2(SO_4)_3$ causes increased coagulation of the RB5 dye. This is because the coagulant ions (Fe^{3+} and Fe^{2+}) can neutralize the anionic form of the RB5 dye. However, when the pH level exceeds 7, there are more OH^- ions available to react with the coagulant ions (SO_4^{2-}, Fe^{2+} and Fe^{3+}) present in the medium to form $Fe(OH)_3$ and $Fe(OH)_2$. These hydroxides are molecules with a large specific surface area with multiple adsorption sites. As a result, there is reduced availability of irons for RB5 coagulation, leading to unsatisfactory outcomes.

Also, it is well established that the type of coagulant influences COD removal, as indicated in Fig. 12. Indeed, the highest level of COD elimination effectiveness as a function of coagulant type follows the following sequence: $Fe_2(SO_4)_3$ (84.71%) > $FeCl_3$ (78.71%) > $Al_2(SO_4)_3$ (67.37%) > $AlCl_3$ (56.25%). A study conducted previously found that a comparable sequence to our investigation was identified for COD removal from wastewater that contains the RB5 dye. ($Fe_2(SO_4)_3$(90 ± 0.002) > $FeCl_3$ (78 ± 0.02) > alum (76 ± 0.006) > PACl (60 ± 0.005) > $FeSO_4$ (20 ± 0.003)) [51].

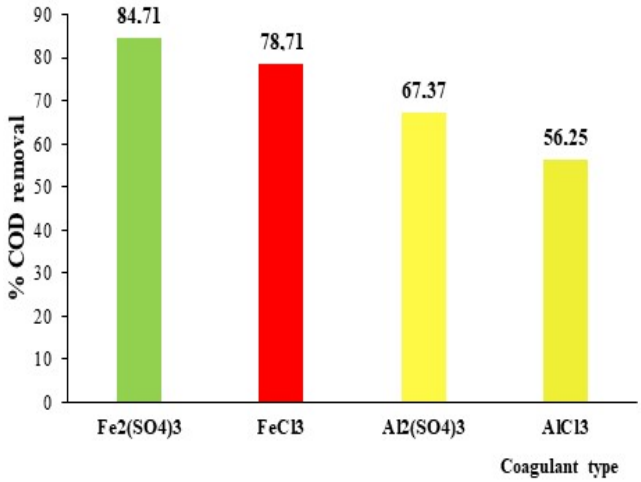

Fig. 12. The effect of the coagulant type on the %COD removal at [coagulant] = 200 mg l^{-1}, [RB5] = 500 mg l^{-1}, and (pH = 4 for $Fe_2(SO_4)_3$ and $FeCl_3$, pH = 6 for $Al_2(SO_4)_3$, and pH = 8 for $AlCl_3$).

In addition, we conducted a comparative analysis of our study's findings with those of other researchers, considering the pH conditions, coagulant dose, and COD removal efficiency (Table 9). Our findings validate that the use of $Fe_2(SO_4)_3$ coagulant is highly effective in removing COD.

As an outcome, the experimental findings are in close concordance with the DFT-conducted study, with a high level

Table 9. Comparison between Actual and Previous Studies

Used dye	Coagulant	pH	CDO Removal	Coagulant dose (mg l^{-1})	Ref.
Effluent RB5 dye	Coagulation-$Fe_2(SO_4)_3$	4	84.71	200	This study
Effluent RB5 dye	Coagulation-$FeCl_3$	4	78.71	200	This study
Textile wastewater	$FeCl_3$	4	54	4000	[52]
Textile wastewater	$FeCl_3$	5	72	550	[53]
Textile wastewater	$Al_2(SO_4)_3$	7	36	550	[53]
Effluent RB5 dye	$Fe_2(SO_4)_3$	4	90	200	[51]
Textile wastewater	$FeCl_3$	9	62.2	1000	[54]

of COD removal recorded by the coagulant $Fe_2(SO_4)_3$ due to its higher level of electron acceptance ($\omega^+ = 9.754$ eV). Thus, its higher electrophilicity ($\omega = 26.063$), the lowest hardness ($\eta = 0.95$ eV), and the highest softness ($S = 1.06$ eV), which explains their higher reactivity with RB5 compared with the other coagulants (Table 5), resulting in strong coagulation of RB5 dye. This could imply a high percentage of dye removal (Fig. 12).

.

CONCLUSION

This study used the Gaussian 09W software to apply density functional theory (DFT/B3LYP) with a 6-31G(d) basis set. This work has been focused on the analysis of the reactivity between reactive black-5 (RB5) dye and ferric sulphate ($Fe_2(SO_4)_3$), ferric chloride ($FeCl_3$), aluminium sulphate ($Al_2(SO_4)_3$), and aluminium chloride ($AlCl_3$) as coagulants. The results revealed that the ranking of the different coagulants based on the electrophilicity index was: $Fe_2(SO_4)_3$ (ω = 26.063 eV) > $FeCl_3$ (ω = 23.713 eV) > $Al_2(S0_4)_3$ (ω = 22.255 eV) > $AlCl_3$ (ω = 6.156 eV). The calculation and analysis of global and local reactivity descriptors of various coagulants have indicated that the coagulant $Fe_2(SO_4)_3$ acts as an electrophile and the RB5 dye ($\omega_k = 2.797$ eV) as a nucleophile. Based on the MEPs diagram, the areas with positive potential have been situated near the sulphur atoms of the $Fe_2(SO_4)_3$ molecule, where there is a higher concentration of protons and fewer electrons. The positive potential sites have been also found around the ferric atom of the $FeCl_3$ molecule. The atoms with electronegative charges (indicated by the color red) are the locations with negative potential. The Parr index calculation P_k^+ and P_k^- of the RB5 dye has demonstrated that the sites most susceptible to nucleophilic attack are those with the highest value of ω_k are on the benzene rings (C5-9H $\omega_k = 2.797$eV, -C1-50N $\omega_k = 2.671$ eV), the nitrogen region (-N79-80H-81H $\omega_k = 1.968$ eV, -N51=N50- $\omega_k = 1.769$ eV) and sulphur (-C52-62S $\omega_k = 1.137$ eV). Similarly, this calculation has shown that the most reactive site in the case of a nucleophilic attack on the RB5 dye is in the C5-9H bonding region (ω_k= 2.797 eV). The experimental results well confirmed the theoretical study, with the $Fe_2(SO_4)_3$ coagulant achieving the highest COD removal rate (84.71% at pH = 4) due to its higher electron acceptance level than the other coagulants, resulting in strong coagulation of RB5, implying a high percentage of dye removal.

This study offers valuable insights into the relevance of implementing DFT in industrial wastewater treatment, specifically in identifying the most efficient coagulant without extensive experimentation. Through computational analysis, we aim to further validate our findings by conducting an empirical investigation using the coagulation-flocculation method to eliminate the reactive Black-5 dye from industrial effluents.

REFERENCES

[1] Pei, S.; Zhao, J., A Scalable Approach Support for External Milk-run Planning and Optimization in Home Appliances Enterprises. Proceedings of the 8 th International Conference on Information Management and Engineering -ICIME-, Istanbul: **2016**, 67-70, DOI: 10.1145/3012258.3012277.

[2] Mansour, H. B.; Boughzala, O.; Dridi, D.; Barillier, D.; Chekir-Ghedira, L.; Mosrati, R., Les colorants textiles sources de contamination de l'eau: Criblage de la toxicité et des méthodes de traitement. *Rev. Sciences de l'eau.* **2011**, *24* (3), 103-327, DOI: 10.7202/1006453ar.

[3] Berradi, M., Textile finishing dyes and their impact on aquatic environs. *Heliyo.* **2019**, *5* (11), e02711, DOI: 10.1016/j.heliyon.2019.e02711.

[4] Mcyotto, F.; Wei, Q.; Macharia, D. K.; Huang, M.; Shen, C.; Chow, C. W. K., Effect of dye structure on color removal efficiency by coagulation. *J. Chem. Eng.* **2021**, *405*, 126674, DOI: 10.1016/ j.cej.2020.126674.

[5] Bhagavathi Pushpa, T.; Vijayaraghavan, J.; Sardhar Basha, S. J.; Sekaran, V.; Vijayaraghavan, K.; Jegan, J., Investigation on removal of malachite green using EM based compost as adsorbent. *Ecotoxicol. Environ. Saf.* **2015**, *118*, 177-182, DOI: 10.1016/ j.ecoenv.2015.04.033.

[6] Yaashikaa, P. R.; Kumar, P. S.; Saravanan, A., Advances in biosorbents for removal of environmental pollutants: A review on pretreatment, removal mechanism and future outlook. *J. Hazard.*

Mater. **2021**, *420*, 126596, DOI: 10.1016/j.jhazmat.2021.126596.

[7] Katheresan, V.; Kansedo, J.; Lau, S. Y., Efficiency of various recent wastewater dye removal methods: A review. *J. Environ. Chem. Eng.* **2018**, *6* (4), 4676-4697, DOI: 10.1016/j.jece.2018.06.060.

[8] Samsami, S.; Mohamadi zaniani, M.; Sarrafzadeh, M. -H.; Rene, E. R.; Firoozbahr, M., Recent advances in the treatment of dye-containing wastewater from textile industries: Overview and perspectives. *Process Saf. Environ. Prot.* **2020**, *143*, 138-163, DOI: 10.1016/j.psep.2020.05.034.

[9] Li. R., Efficient decolorization of azo dye wastewater with polyaniline/graphene modified anode in microbial electrochemical systems. *J. Hazard. Mater.* **2022**, *421*, 126740, DOI: 10.1016/j.jhazmat.2021.126740.

[10] Abbasi, S.; Mirghorayshi, M.; Zinadini, S.; Zinatizadeh, A. A., A novel single continuous electrocoagulation process for treatment of licorice processing wastewater: Optimization of operating factors using RSM. *Process Saf. Environ. Prot.* **2022**, *134*, 323-332, DOI: 10.1016/j.psep.2019.12.005.

[11] Boczkaj, G.; Fernandes, A., Wastewater treatment by means of advanced oxidation processes at basic pH conditions: A Review. *Chem. Eng. J.* **2017**, *320*, 608-633, DOI: 10.1016/j.cej.2017.03.084.

[12] Ibrahim, S. M.; Al-Hossainy, A. F., Synthesis, structural characterization, DFT, kinetics and mechanism of oxidation of bromothymol blue: application to textile industrial wastewater treatment. *Chem. Pap.* **2021**, *75* (1), DOI: 10.1007/s11696-020-01299-8.

[13] Junejo, R.; Shams Jalbani, N.; Kaya, S.; Serdaroglu, G.; Şimşek, S.; Memon, S., Experimental and DFT Modeling Studies for the Adsorptive Removal of Reactive Dyes from Wastewater. *Sci. Technol.* **2021**, *57* (3), 1-15, DOI: 10.1080/01496395.2021.1900252.

[14] Ghafari, S.; Aziz, H. A.; Isa, M. H.; Zinatizadeh, A. A., Application of response surface methodology (RSM) to optimize coagulation–flocculation treatment of leachate using poly- aluminum chloride (PAC) and alum. *J. Hazard. Mater.* **2016**, *163*, 2-3, DOI: 10.1016/j.jhazmat.2008.07.090.

[15] Sabur, M. A.; Khan, A. A.; Safiullah, S., Treatment of Textile Wastewater by Coagulation Precipitation Method. *J. Sci. Res.* **2012**, *4* (3), DOI: 10.3329/jsr.v4i3.10777.

[16] Sherrill, C. D., Frontiers in electronic structure theory. *J. Chem. Phys.* **2010**, *132* (11), 110902, DOI: 10.1063/1.3369628.

[17] Domingo, L. R.; Aurell, M. J.; Pérez, P.; Contreras, R., Quantitative Characterization of the Local Electrophilicity of Organic Molecules. Understanding the Regioselectivity on Diels-Alder Reactions. *J. Phys. Chem. A*, **2002**, *106* (29), DOI: 10.1021/jp020715j.

[18] Domingo, L. R.; Pérez, P.; Contreras, R., Reactivity of the carbon-carbon double bond towards nucleophilic additions. A DFT analysis. *Tetrahedron*. **2004**, *60* (31), DOI: 10.1016/j.tet.2004.06.003.

[19] Domingo, L. R.; Ríos-Gutiérrez, M.; Pérez, P., Applications of the Conceptual Density Functional Theory Indices to Organic Chemistry Reactivity. *Molecules*. **2016**, *21* (6,), DOI: 10.3390/molecules21060748.

[20] Regti, A.; Ayouchia, H. B. E.; Laamari, M. R.; Stiriba, H.; Haddad, M. E., Experimental and theoretical study using DFT method for the competitive adsorption of two cationic dyes from wastewaters. *Appl. Surf. Sci.* **2016**, *390*, 311-319, DOI: 10.1016/j.apsusc.2016.08.059.

[21] Achour, Y.; Khouili, M.; Abderrafia, H.; Melliani, S.; Laamari, M. R.; El Haddad, M., DFT Investigations and Experimental Studies for Competitive and Adsorptive Removal of Two Cationic Dyes onto an Eco-friendly Material from Aqueous Media. *Int. J. Environ. Res.* **2018**, *12* (6), DOI: 10.1007/s41742-018-0131-x.

[22] El Haouti, R.; Ouachtak, H.; El Guerdaoui, A.; Amedlous, A.; Amaterz, E.; Haounati, R.; Ait Addi, A.; Akbal, F.; El Alem, N.; Labd Taha, M., Cationic dyes adsorption by Na-Montmorillonite Nano Clay: Experimental study combined with a theoretical investigation using DFT-based descriptors and molecular dynamics simulations. **2019**, *290*, 111-139, DOI: 10.1016/j.molliq.2019.111139.

[23] Elhorri, A. M.; Belaid, K. D.; Zouaoui-Rabah, M.;

Chadli, R., Theoretical study of the azo dyes dissociation by advanced oxidation using Fukui indices. DFT calculations. *Comput. Theor. Chem.* **2018**, *1130*, 98-106, DOI: 10.1016/ j.comptc.2018.03.018.

[24] El Kassimi, A.; Boutouil, A.; El Himri, M.; Rachid Laamari, M.; El Haddad, M., Selective and competitive removal of three basic dyes from single, binary and ternary systems in aqueous solutions: A combined experimental and theoretical study. *J. Saudi Chem. Soc.* **2020**, *24* (7), DOI: 10.1016/ j.jscs.2020.05.005.

[25] Wong, C.; Lai, C.; Lee, K.; Hamid, S., Advanced Chemical Reduction of Reduced Graphene Oxide and Its Photocatalytic Activity in Degrading Reactive Black 5. *Materials*. **2015**, *8* (10), 7118-7128, DOI: 10.3390/ma8105363..

[26] Guillaumont, D.; Nakamura, S., Calculation of the absorption wavelength of dyes using time-dependent density-functional theory (TD-DFT). *Dyes Pigments.* **2000**, *46*, 85-92, DOI: 10.1016/S0143-7208(00)00030-9.

[27] Frisch, M. J. T.; Schlegel, G. W.; Scuseria, H. B.; Robb, G. E.; Cheeseman, M. A.; Scalmani, J. R.; Barone, G.; Mennucci, V.; Petersson, B.; Nakatsuji. G. A., vol. Revision D. 01. Wallingford CT: Gaussian. Inc., **2009**.

[28] Zhao, Y.; Truhlar, D. G., Hybrid Meta Density Functional Theory Methods for Thermochemistry, Thermochemical Kinetics, and Noncovalent Interactions: The MPW1B95 and MPWB1K Models and Comparative Assessments for Hydrogen Bonding and van der Waals Interactions. *J. Phys. Chem. A.* **2004**, *108* (33), 6908-6918, DOI: 10.1021/jp048147q.

[29] Chaair, H.; Driouich, A.; alami El hassani, S. E.; Chajri, F.; Britel, O.; Digua, K., Synthesis and Characterization of Silicate Gel by using Sol-gel Process: Experiments and DFT calculations. *Mediterr. J. Chem.* **2020**, *9* (6), 411-421, DOI: 10.13171/ mjc9602001011134hc.

[30] El Nemr, A.; Moneer, A. A.; Khaled, A., El Sikaily, A.; El-Said, G. F., Modeling of synergistic halide additives' effect on the corrosion of aluminum in basic solution containing dye. *Mater. Chem. Phys.*, **2014,** *144*, 139-154, DOI: 10.1016/ j.matchemphys.2013.12.034.

[31] Gázquez, J. L.; Cedillo, A.; Vela, A., Electrodonating and Electroaccepting Powers. *J. Phys. Chem. A.* **2007**, *111* (10), 1966-1970, DOI: 10.1021/jp065459f.

[32] Belghiti, M. E.; Bouazama, S.; Echihi, S.; Mahsoune, A.; Elmelouky, A.; Dafali, A.; Emran, K. M.; Hammouti, B.; Tabyaoui, M., Understanding the adsorption of newly Benzylidene-aniline derivatives as a corrosion inhibitor for carbon steel in hydrochloric acid solution: Experimental, DFT and molecular dynamic simulation studies. *Arab. J. Chem.* **2017**, *13* (1), DOI: 10.1016/j.arabjc.2017.12.003.

[33] Pearson, R. G, Chemical Hardness. Wiley-VCH Verlag GmbH, Weinheim, **1997**, 29-58, DOI: 10.1002/3527606173.ch2.

[34] Islam, N.; Ghosh, D. C., On the Electrophilic Character of Molecules Through Its Relation with Electronegativity and Chemical Hardness. *Int. J. Mol. Sci.* **2012**, *13*, 2160-2175, doi: 10.3390/ ijms13022160.

[35] Lesar, A.; Milošev, I., Density functional study of the corrosion inhibition properties of 1,2,4-triazole and its amino derivatives. *Chem. Phys. Lett.* **2009**, *483* (6), 198-203, DOI: 10.1016/j.cplett.2009.10.082.

[36] Parr, R. G.; Szentpály, L. V.; Liu, S., Electrophilicity Index. *J. Am. Chem. Soc.* **2017**, 12519, DOI: 10.1021/ja983494x.

[37] Domingo, L. R.; Sáez, J. A., Understanding the mechanism of polar Diels-Alder reactions. *Org. Biomol. Chem.* **2009**, *7* (17), DOI: 10.1039/b909611f.

[38] Domingo, L. R.; Chamorro, E.; Pérez, P., Understanding the Reactivity of Captodative Ethylenes in Polar Cycloaddition Reactions. A Theoretical Study. *J. Org. Chem.* **2008**, *73* (12), DOI: 10.1021/jo800572a.

[39] Domingo L. R.; Pérez, P., The nucleophilicity N index in organic chemistry. *Org. Biomol. Chem.* **2019**, *9* (20), DOI: 10.1039/c1ob05856h.

[40] Kohn, W.; Sham, L. J., Self-Consistent Equations Including Exchange and Correlation Effects. *Phys. Rev.* **1965**, *140* (4), 1133-1138, DOI: 10.1103/ PhysRev.140.A1133.

[41] El Kassimi, A.; Achour, Y.; El Himri, M.; Laamari,

R.; El Haddad, M., Removal of two cationic dyes from aqueous solutions by adsorption onto local clay: experimental and theoretical study using DFT method. *Int. J. Environ. Anal. Chem.* **2021**, 1-22. DOI: 10.1080/03067319.2021.1873306.

[42] Barhoumi, A.; El idrissi, M.; Bakkas, S.; Zeroual, A.; Tounsi, A.; El Hajbi, A., A DFT study of the mechanism and regioselectivity of the reaction between diethyl trichloro-methyl phosphonate and diphenyl methyl phosphinite. *Mor. J. Chem.* **2020**, *8* (4), 12, DOI: 10.48317/IMIST.PRSM/morjchem-v8i4.20720.

[43] Barhoumi, A.; El Idrissi, M.; Zeroual, A.; Tounsi, A.; Bakkas, S.; El Hajbi, A., Theoretical study of the chemical reactivity of a class of trivalent phosphorus derivatives towards polyhaloalkanes: DFT study. *J. Mol. Model.* **2021**, *27* (7), 197, DOI: 10.1007/s00894-021-04814-0.

[44] Ramesh, G.; Reddy, B. V., Spectroscopic investigation on structure (monomer and dimer), molecular characteristics and comparative study on vibrational analysis of picolinic and isonicotinic acids using experimental and theoretical (DFT & IVP) methods. *J. Mol. Struct.*, **2018**, *1160*, 271-292, DOI: 10.1016/j.molstruc.2018.01.083.

[45] Khajehzadeh, M.; Sadeghi, N., Molecular structure, X-ray crystallography, spectroscopic characterization, solvent effect, NLO, NBO, FMO analysis of [Cu(bpabza)] complexe. *J. Mol. Liq.* **2018**, 249, 281-293, DOI: 10.1016/j.molliq.2017.10.142.

[46] Reed, A. E.; Weinhold, F., Natural bond orbital analysis of near-Hartree-Fock water dimer. *J. Chem. Phys.* **1983**, *78*, 4066-4073, DOI: 10.1063/1.445134.

[47] Pérez, P.; Domingo, L. R.; Duque-Noreña, M.; Chamorro, E., A condensed-to-atom nucleophilicity index. An application to the director effects on the electrophilic aromatic substitutions. *J. Mol. Struct. Theochem.* **2009**, *895* (1), 86-91, DOI: 10.1016/ j.theochem.2008.10.014.

[48] Domingo, L. R.; Pérez, P.; Sáez, J. A., Understanding the local reactivity in polar organic reactions through electrophilic and nucleophilic Parr functions. *RSC Adv.* **2013**, *3* (5), DOI: 10.1039/C2RA22886F.

[49] Domingo, L. R.; Pérez, P.; Contreras, R., Reactivity of the carbon-carbon double bond towards nucleophilic additions. *A DFT Analysis. Tetrahedron.* **2004**, *60* (31), 6585-6591, DOI:10.1016/j.tet.2004.06.003.

[50] Sinha, S.; Yoon, Y.; Amy, G.; Yoon, J., Determining the effectiveness of conventional and alternative coagulants through effective characterization schemes. *Chemosphere.* **2004**, *57* (9), 1115-1122, DOI: 10.1016/j.chemosphere.2004.08.012.

[51] Tlaiaa, Y. S.; Razaq Naser, Z. A.; Ali, A. H., Comparison between coagulation and electrocoagulation processes for the removal of reactive black dye RB-5 and COD reduction. Desalination and Water Treatment. **2020**, (195), 154-161, DOI: 10.5004/dwt.2020.25914.

[52] Rana, S.; S. Suresh. Comparison of Different Coagulants for Reduction of COD from Textile Industry Wastewater. Materials Today: Proceedings. **2017**, *4* (2), 567-574, https://doi.org/10.1016/j.matpr.2017.01.058.

[53] Naghan, D. J.; Motevalli, M. D.; Mirzaei, N.; Javid, A.; Ghaffari, H. R.; Ahmadpour, M.; Moradi, M.; Sharafi, K., Efficiency Comparison of Alum and Ferric Chloride Coagulants in Removal of Dye and Organic Material from Industrial Wastewater-a Case Study. Bulgarian Chemical Communications. **2015**, *47*, 206-210.

[54] Karam, A.; Bakhoum, E. S.; Khaled Zaher, Z., Coagulation/flocculation process for textile mill effluent treatment: experimental and numerical perspectives, *International Journal of Sustainable Engineering.* **2021**, *14* (5), 983-995, DOI: 10.1080/19397038.2020.1842547.